Title
Dynamics of Metastable β-Hairpin Structures in the Folding Nucleus of Amyloid β-Protein

Journal
The Journal of Physical Chemistry B, 116(22)

ISSN
1520-6106

Authors
Cruz, L
Rao, J Srinivasa
Teplow, DB
et al.

Publication Date
2012-06-07

DOI
10.1021/jp301619v

Peer reviewed

THE JOURNAL OF PHYSICAL CHEMISTRY B

Article

pubs.acs.org/JPCB

Dynamics of Metastable β-Hairpin Structures in the Folding Nucleus of Amyloid β-Protein

L. Cruz,*[,†] J. Srinivasa Rao,[†] D. B. Teplow,[‡] and B. Urbanc[†]

[†]Department of Physics, 3141 Chestnut Street, Drexel University, Philadelphia, Pennsylvania 19104, United States

[‡]Department of Neurology, David Geffen School of Medicine at UCLA; Mary S. Easton Center for Alzheimer's Disease Research at UCLA; and Molecular Biology Institute and Brain Research Institute, UCLA, Los Angeles, Los Angeles, California 90095, United States

Supporting Information

ABSTRACT: The amyloid β-protein (Aβ), which is present predominately as a 40- or 42-residue peptide, is postulated to play a seminal role in the pathogenesis of Alzheimer's disease (AD). Folding of the Aβ_{21-30} decapeptide region is a critical step in the aggregation of Aβ. We report results of constant temperature all-atom molecular dynamics simulations in explicit water of the dynamics of monomeric Aβ_{21-30} and its Dutch [Glu22Gln], Arctic [Glu22Gly], and Iowa [Asp23Asn] isoforms that are associated with familial forms of cerebral amyloid angiopathy and AD. The simulations revealed a variety of loop conformers that exhibited a hydrogen bond network involving the Asp23 and Ser26 amino acids. A population of conformers, not part of the loop population, was found to form metastable β-hairpin structures with the highest probability in the Iowa mutant. At least three β-hairpin structures were found that differed in their hydrogen bonding register, average number of backbone hydrogen bonds, and lifetimes. Analysis revealed that the Dutch mutant had the longest β-hairpin lifetime ($\geq$500 ns), closely followed by the Iowa mutant ($\approx$500 ns). Aβ_{21-30} and the Arctic mutant had significantly lower lifetimes ($\approx$200 ns). Hydrophobic packing of side chains was responsible for enhanced β-hairpin lifetimes in the Dutch and Iowa mutants, whereas lifetimes in Aβ_{21-30} and its Arctic mutant were influenced by the backbone hydrogen bonding. The data suggest that prolonged β-hairpin lifetimes may impact peptide pathogenicity *in vivo*.

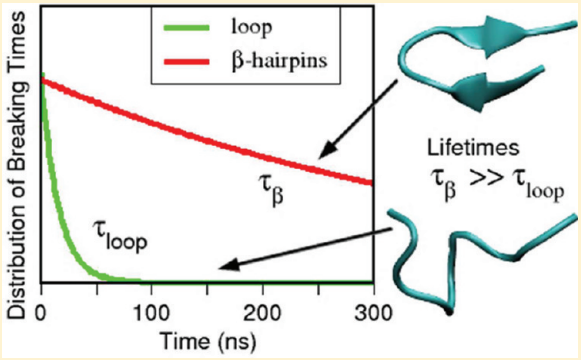

INTRODUCTION

Alzheimer's disease (AD) is a progressive, age-associated, neurological disorder that is rapidly reaching epidemic proportions. The pathognomonic signs of AD are extracellular amyloid plaques and intraneuronal neurofibrillary tangles that are composed of the amyloid β-protein (Aβ) and tau protein, respectively. Progression of AD is associated with profound neuronal loss, the precise cause of which remains enigmatic. Historically, amyloid plaques were thought to cause AD.[1−4] However, accumulating evidence suggests that the dominant neurotoxins in AD are oligomeric forms of Aβ.[5−13] If so, then understanding the mechanisms of the toxicity of Aβ oligomers holds therapeutic potential.

Achieving this understanding requires the determination of the structures of the toxins and a correlation of structure with neurotoxicity. Experimental and computational studies have addressed possible mechanisms of Aβ folding and oligomer formation for both full-length alloforms, Aβ_{1-40} and Aβ_{1-42} (e.g., refs 9 and 14 and references therein). Precise experimental determination of the structure of low-order oligomers, and even the monomer, has proven to be difficult because Aβ belongs to the class of intrinsically disordered proteins.[15,16] Even partially ordered Aβ conformers are transient and unstable.[17,18] A zero-length chemical cross-linking approach has enabled the stabilization of Aβ_{1-40} oligomers, the isolation of pure Aβ_{1-40} monomers, dimers, trimers, and tetramers, and the determination of order-specific neurotoxicity.[19] In general, the tendency of Aβ to aggregate makes experimental studies particularly difficult.[20−23] For this reason, many experimental and computational studies have focused on fragments of Aβ that preserve key properties of the full-length alloforms while aggregating less rapidly.[24−36] This preservation of structure in fragments, however, is not universal.[37]

An important fragment is the Aβ_{21-30} decapeptide. Using limited proteolysis and solution NMR, Lazo et al.[38] have shown that this region within both Aβ_{1-40} and Aβ_{1-42} monomers is protease-resistant. Surprisingly, the isolated decapeptide also is protease resistant, suggesting that it functions as an Aβ monomer folding nucleus. Subsequent computational studies revealed the presence of bends or loops stabilized by hydrophobic packing between side chains of Val24 and Lys28.[39−42] A combined experimental and computational

Received: February 18, 2012
Revised: April 20, 2012
Published: May 15, 2012

   dx.doi.org/10.1021/jp301619v | J. Phys. Chem. B 2012, 116, 6311−6325

study using solution NMR and replica exchange MD (REMD) simulations concluded that the Aβ_{21-30} fragment existed mostly (but not entirely) in unstructured conformations, lacking any secondary structure or persistent hydrogen bonding (HB) network but showing evidence for an Asp23−Lys28 salt bridge (SB) formation that could stabilize the Aβ fibril structure.[43] Intriguingly, a minority population of conformers contained a β-turn centered at Val24−Gly25.

Further clues to the mechanistic bases of Aβ-induced disease come from families in which mutations in the structural gene for Aβ, the amyloid β-protein precursor gene (APP), cause familial forms of AD (FAD) and cerebral amyloid angiopathy (CAA). In these cases, a number of single amino acid mutations within Aβ at positions 22 and 23 result in more aggressive forms of AD and *in vitro* aggregate more readily than the wild type (WT) Aβ. Examples include the Arctic [Glu22Gly], Dutch [Glu22Gln], and Iowa [Asp23Asn] mutants.[44−50] Experimental and computational studies on Aβ_{21-30} decapeptides containing these amino acid substitutions showed that the turn in the Val24−Lys28 region was destabilized, which resulted in intramolecular interactions between the Aβ_{21-30} region and the rest of the full-length peptide that may facilitate oligomerization and fibril formation.[51] A follow-up computational study suggested that mutations at position 23 produced peptide conformers different from those produced by mutations at position 22.[52] Ion mobility spectrometry coupled with computational studies further found that a HB network involving Asp23 contributed substantially to turn formation and stability, suggesting that mutations at position 23 (Iowa) led to significant structural changes, whereas mutations at position 22 ([Glu22Gln], [Glu22Gly], [Glu22Lys]) led to only subtle variations to the overall folded structure of Aβ_{21-30}.[53]

In the Aβ system, folding units observed in the Aβ monomer or subregions thereof can be maintained in higher-order assemblies. Solid state NMR of fibrils formed by full-length Aβ_{1-40} showed that the fibrils comprise two β-strand regions (12−24 and 30−40) connected by a bend in the 25−29 region. This bend brought the two β-strands together to form parallel β-sheets through side chain−side chain interaction.[54,55] Several computational studies of full-length Aβ showed significant structure, such as β-strands, in several regions of the peptide, with some of them spanning the 21−30 decapeptide region.[56−62] However, other studies did not report any β-structure.[63,64]

Additional experimental studies supported the importance of the 21−30 peptide turn in controlling aggregation propensity. Aβ_{1-40} with a lactam (Asp23/Lys28) bridge showed that such a preformed bend/turn increased fibrillogenesis by a factor of 1000 relative to the WT peptide.[65] Also, by forming a disulfide bond between amino acids 21 and 30 (using cysteine substitutions: [Ala21Cys] and [Ala30Cys]), full-length Aβ monomers formed a β-hairpin with strands comprising amino acids 17−23 and 30−36 that resulted in toxic oligomeric species.[66] Interestingly, this disulfide bond prevented further assembly of these oligomers into amyloid fibrils, suggesting that if there was structure in the unmodified 21−30 decapeptide region that initially forms and nucleates the folding of the Aβ, this structure was metastable. If an intermediate, but benign, structure within the 21−30 decapeptide region could be stabilized, this would be a new therapeutic option, as it could destabilize a potentially toxic state.[67] A recent study has shown that maintenance of a benign conformational state in the transthyretin tetramer may be an effective strategy for treating diseases like familial amyloid polyneuropathy or systemic amyloidosis.[68]

Here, using constant temperature all-atom MD in explicit water, the dynamics of Aβ_{21-30} and its Dutch, Arctic, and Iowa mutants was examined. The decapeptide structural landscape comprises a variety of loop structures and at least three types of metastable β-hairpins. Differences in the structure and lifetimes of these metastable β-hairpins were observed among the four different decapeptides. These different β-hairpins could play a critical role in nucleating full-length Aβ folding, while the differences in structure and lifetimes reported here could be responsible for distinct folding pathways and aggregation propensity for each of these decapeptides.

METHODS

MD Simulations. Long-time constant temperature MD simulations of the decapeptide Aβ_{21-30} monomer in explicit TIP4P[69] water were performed. All atoms were explicitly considered with potential energies given by the OPLS/AA[70] force field within the GROMACS 4.0.5[71,72] package and using the NPT ensemble.[73] The system was confined in a cubic box with periodic boundary conditions. MD simulations were carried out at a constant temperature of T = 283 K corresponding to *in vitro* experiments.[38] In the simulations, amino acids were numbered sequentially starting from Ala21 through Ala30, corresponding to position 21 through 30 of the full length amyloid β-protein. The WT Aβ_{21-30} had the primary structure Ala-Glu-Asp-Val-Gly-Ser-Asn-Lys-Gly-Ala, where Glu22 and Asp23 were negatively charged and Lys28 was positively charged. Following Lazo et al,[38] the Aβ_{21-30} was blocked with NH_3^+ and CO_2^- at the N^- and C^- termini, respectively. Simulations with the Arctic [Glu22Gly], Dutch [Glu22Gln], and Iowa [Asp23Asn] mutations were also considered. In each case, the peptide was initially solvated by inserting it in the center of a previously equilibrated cube of water molecules of side 43 Å. This insertion deleted all water molecules overlapping or in close proximity (<2.4 Å) to any of the monomer atoms, resulting in a system with an approximate number of water molecules of 2500. To maintain system neutrality (for WT only), a single Na^+ ion was inserted far from the peptide.

The SETTLE algorithm[74] was used to hold constant the covalent bonds of the water molecules. The bonds involving hydrogens were constrained according to the LINCS protocol.[75] Neighbor lists updated every 10 simulation steps were used for the nonbonded interactions. To calculate the electrostatic interactions, a particle mesh Ewald method[76] was used with a cutoff distance of 10 Å for nonbonded interactions and a 1.2 Å grid spacing for the Fourier transform in the reciprocal space for all trajectories. A time step of 2 fs was used in all trajectories. The temperature was controlled by coupling the system to an external bath.[73,77] The energy of the system was first minimized for 20 000 steps by applying the conjugate gradient algorithm that relaxed all atoms except the C_α atoms. Next, the C_α atoms were released and minimized again for another 20 000 steps. The system was gradually heated in the NVT ensemble from 0 to 283 K by harmonically constraining all C_α atoms for 100 ps. Following this step, and still constraining the C_α atoms, another 200 ps were performed in the NPT ensemble at 283 K and 1 atm, followed by a brief 50 ps NPT simulation with no constraints to generate the starting configuration for the production runs. Because of the way that the overlapping water molecules were deleted in the solvation

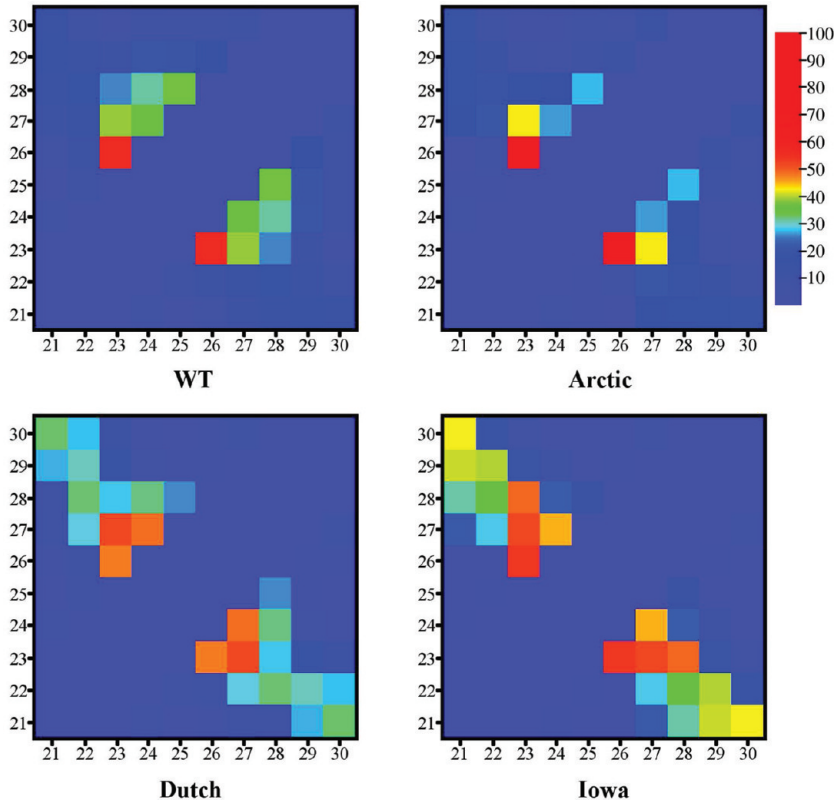

Figure 1. Contact maps for the WT (upper left), Arctic (upper right), Dutch (lower left), and Iowa (lower right) mutants where the colors represent the percentage of the trajectory containing each contact. A contact was established whenever the distance between C_α–C_α atoms of different amino acids fell below 7 Å. In each map, the lower left corner indicates the Ala21–Ala21 contact while the upper right corner indicates the Ala30–Ala30 contact. The color bar on the right indicates the conversion between the color of the contact and the trajectory percentage for that contact.

step above, these NPT equilibration steps allowed for water molecules to fill in holes left from the insertion of the decapeptide, thus shrinking the size of the system by about 1 Å in all directions.

To study the dynamics of the WT decapeptide, 34 trajectories were generated with total running times between 100 and 300 ns, resulting in 8.8 μs of total simulation time. The initial conformations for these trajectories were selected from previously generated stretched chain conformations (conformations with large R_g). Water molecules were given different velocities in each trajectory (based on a Maxwell velocity distribution), making the trajectories independent of each other. The number of trajectories for each of the mutant peptides, which were initially in a stretched chain conformation, was as follows: (i) seven trajectories for the Arctic mutant, resulting in 710 ns, (ii) seven trajectories for the Dutch mutant, resulting in 700 ns, and (iii) eight trajectories for the Iowa mutant, resulting in 900 ns of simulation time. These trajectories had total running times between 100 and 200 ns each.

Trajectories to estimate lifetimes of β-hairpin structures (described below) were carried out starting from the preformed β-hairpin under consideration. The time at which this β-hairpin would unfold was taken as the *breaking time*, τ_i, for that trajectory labeled *i*. A total of 10 trajectories per β-hairpin conformation were performed for each of the four variants (WT, Arctic, Dutch, and Iowa), resulting in 120 additional trajectories. Because these unfolding events were independent of each other, individual values for τ_i were the result of a Poisson process in which state A (β-hairpin) could change into state B (unstructured) with a constant probability per unit time, with τ_i belonging to an exponential distribution. Each β-hairpin lifetime was thus given by the characteristic time of an exponential fit to the distribution of all breaking times $\{\tau_i\}$. To minimize error, the fitting was performed by finding distributions of breaking times $\{\tau_i\}$ using 3–7 bins. This produced five distributions for which exponential fits yielded five corresponding lifetimes. The lifetime for each β-hairpin was then obtained by averaging these five individual lifetimes and obtaining standard deviations. Because each trajectory would be carried out until its β-hairpin structure unfolded, total trajectory times varied but remained in the range from 100 to 400 ns. In less than 6% of the trajectories, β-hairpin structures did not unfold at the 400 ns maximum trajectory length. The total accumulated simulation time for this β-hairpin lifetime analysis amounted to 16.5 μs. Additionally, one replica-exchange MD simulation was performed to test the stability of the β_{28} hairpin conformation (see the Supporting Information), amounting to 1.2 μs of total accumulated running time.

In total, this paper presents data derived from more than 28.8 μs in simulated trajectory times when considering all trajectories used to study the extended conformations and β-hairpin simulation trajectories.

Structural Determinants. To quantify average structures of the decapeptides, contact maps were constructed by counting the number of C_α–C_α distances between different pairs of amino acids that would fall below 7 Å (creating a contact) and dividing this number by the total number of frames in the trajectories. Similarly, HB contact maps were calculated by counting the number of particular HBs and

dx.doi.org/10.1021/jp301619v | J. Phys. Chem. B 2012, 116, 6311–6325

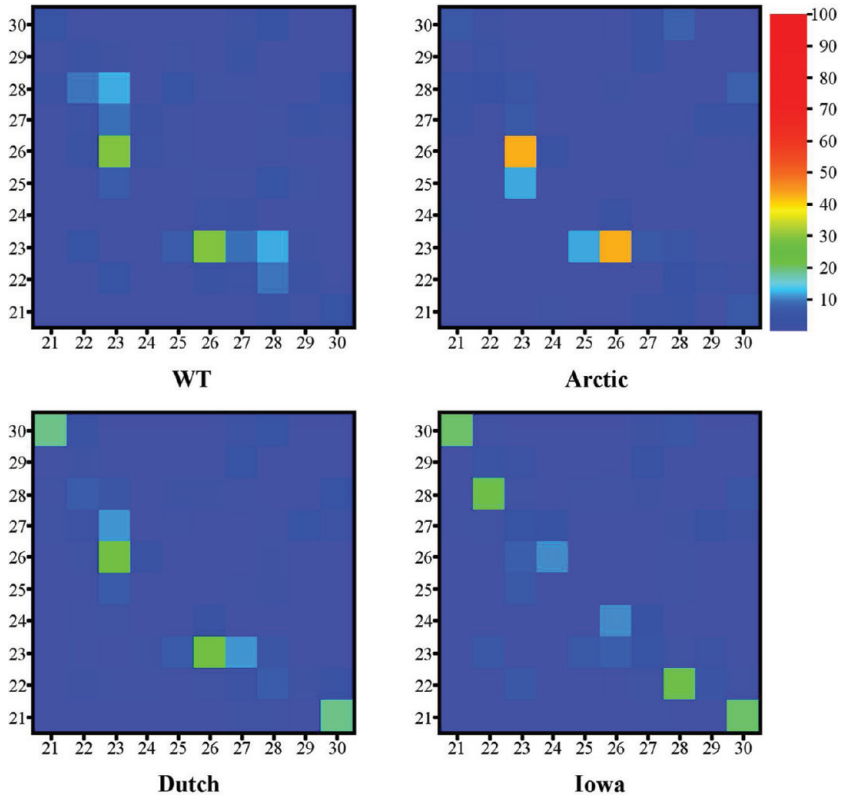

Figure 2. HB contact maps for the WT (upper left), Arctic (upper right), Dutch (lower left), and Iowa (lower right) mutants. The scale on the right indicates the conversion between the color and percentage that each pair of amino acids are connected by HBs.

dividing by the total length of simulations. A HB was defined if the distance between the donor and acceptor was $\leq$3 Å and the angle θ between the donor−hydrogen−acceptor atoms was in the range $160° \geq \theta \leq 200°$. If, in addition, two hydrogen-bonded atoms were of opposite charges, they formed a SB.[78]

To quantify changes in structure of the decapeptide as a function of time, the radius of gyration R_g and specific distances between atoms were measured and labeled using the notation $R(x,y)$, where R was the distance between amino acid x and amino acid y at a particular time.[41] The distances that were taken into consideration were the following: (i) $R(4,8)$ and $R(3,6)$, the distances between the two C_α atoms of Val24 and Lys28 and Asp23 and Ser26, respectively; (ii) $R(2,8)$, the distance between Lys28(N_ζ) and Glu22(C_δ); and (iii) $R(3,8)$, the distance between Lys28(N_ζ) and Asp23(C_δ).

The combined solvent accessible surface areas (SASAs), $S(x,y)$, between amino acids x and y[79] were calculated to monitor for hydrophobic contact formation using the VMD package.[80] Of particular importance was $S(4,8)$, the combined SASA of the Val24 and Lys28 side chains, the $S(3,6)$, $S(3,7)$, and $S(2-4,6-8)$. The $S(2-4,6-8)$ represented the total SASA of the decapeptide excluding the glycines and the terminal alanines. The secondary structure propensity per amino acid was calculated by using the program STRIDE[81] within VMD. The quantity D, used to measure correlations between relative orientations of side chains of two amino acids, was obtained by calculating the normalized scalar product between the vectors defined by the direction of the side chains of Val24 and Lys28.[41]

To find representative conformations from a trajectory, a cluster algorithm based on the matrix of RMSDs as a measure of the distance between two peptide conformations was used.[82] In this algorithm, a representative conformation was found by first measuring all mutual distances (defined by their RMSD distance) between conformations. Given an upper cutoff for this distance, neighborhoods of common conformations were defined and the one with the largest number of conformations selected. Within this selected neighborhood (cluster), the central structure (centroid) was chosen as a representative conformation. This entire neighborhood of conformations was then removed from the pool of conformations, and the algorithm was repeated. In the present work, RMSDs were measured only taking into account the backbone C_α atoms of amino acids 22−28. A cluster was defined as that in which neighboring conformations had an RMSD equal or less than 1 Å.

RESULTS

We first present distance and HB contact maps for each decapeptide variant, which are used to identify the main (whole-trajectory average) structural elements of the four decapeptides. Spontaneously formed, metastable, β-hairpin structures appearing in the trajectories are then characterized using secondary structure and hydrogen bonding analyses. Finally, the lifetimes of these β-hairpin structures are obtained and discussed in terms of hydrophobicity, electrostatic interactions, and hydrogen bonding.

Common Folding Structure of Aβ_{21-30} and Its Mutants. In Figure 1, contact maps between pairs of C_α atoms are shown for the WT and mutant decapeptides. The values of the contacts were calculated as the percentage of the trajectory over which the $C_\alpha-C_\alpha$ distance between amino acids was less than 7 Å. These maps showed that contacts between Asp23 and other inner amino acids (Ser26 and Asn27) were

dx.doi.org/10.1021/jp301619v | J. Phys. Chem. B 2012, 116, 6311−6325

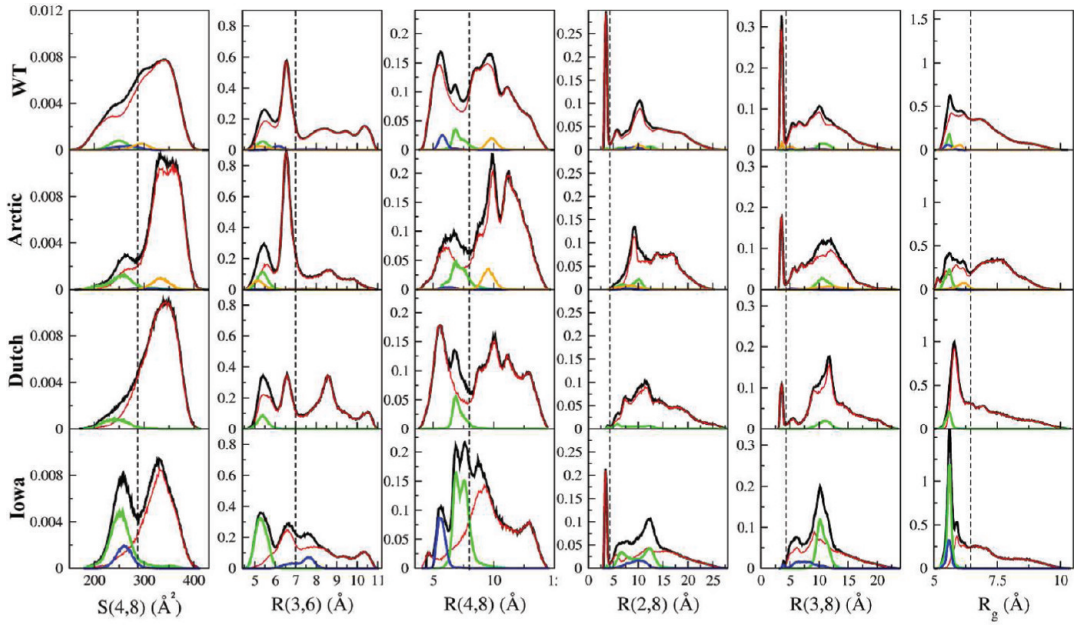

Figure 3. Normalized histograms of $S(4,8)$, amino acid distances $R(x,y)$, and radius of gyration R_g per mutation. Black lines correspond to each quantity calculated using entire trajectories, while blue, green, and orange lines are the individual contributions to the histograms from the β_{28}, β_{29}, and β_{18} hairpins, respectively. The red lines correspond to the histograms calculated excluding the β-hairpins. The dashed vertical lines used to demarcate regions in $S(4,8)$, $R(3,6)$, $R(4,8)$, $R(2/3,8)$, and R_g are at 287 Å^2, 7 Å, 8 Å, 4.2 Å, and 6.3 Å, respectively.

the most prevalent (strongest) for all decapeptide types, suggesting that interactions in the interior of the decapeptides might play a pivotal role in the decapeptide structure. The next four strongest contacts were Gly25−Lys28, Asp23−Lys28, Val24−Asn27, and Ala21−Ala30 (see Table A in the Supporting Information for specific values). Schematic diagrams in Figure I in the Supporting Information illustrate the location and strength of these contacts. The diagonal feature in the contact map of the Iowa mutant (Figure 1) is indicative of a β-hairpin structure and is discussed below. These data show strong contacts between the inner amino acid C_α atoms that reflected a persistent unstructured turn or loop in the central region in all decapeptide variants.

Next, hydrogen bonds between pairs of amino acids were analyzed. Figure 2 shows HB contact maps for all decapeptide types where each contact was calculated as the percentage occurrence of the contacts between pairs of amino acids (strongest HBs are listed in Table B in the Supporting Information). Similarly to Figure 1, the Asp23−Ser26 HB contact was very prominent in the WT, Arctic, and Dutch decapeptides. In the Iowa mutant, however, the dominant HB contact was Glu22−Lys28. Because the Iowa mutant is the only one without a charge at position 23, this result suggested that the absence of charge at position 23 facilitated HB formation. This point was more clearly illustrated when examining specific pairs of atoms forming the HBs (Table C, Supporting Information). The prevalent HBs for the WT, Arctic, and Dutch decapeptides formed between Asp23(O_δ)−Ser26(H) and Asp23(O_δ)−Ser26(H_γ), unlike in the Iowa mutant. Furthermore, the accumulated percentage of HBs for the WT, Arctic, and Dutch mutants involving the charged Asp23(O_δ) were 54, 62.7, and 46.2%, respectively (Table C, Supporting Information). For the Iowa mutant, the total percentage of HBs formed by the uncharged Asn23(O_δ) was only 9.1%. It is important to note that the absence of charge at position 23 in the Iowa mutant was not compensated by an increase of HB propensity of the charged Glu22(O_ε) and formation of the Glu22(O_ε)−Lys28(H_ζ) SB but rather by an increased number of backbone HBs. Thus, the absence of charge at position 23 (as exemplified by the Iowa mutant) but not at position 22 (as exemplified by the Arctic and Dutch mutants) changed the HB network and dynamics.

Analysis of the average secondary structure of each amino acid over the entire trajectories revealed a turn between positions 23 and 27 and unstructured N- and C-termini (Figure II, Supporting Information), consistent with the contact maps (Figures 1 and 2) that indicated persistent bonding among inner amino acids for all decapeptide variants. In addition, there was a small but statistically significant extended β structure involving amino acids at positions 22/23 and 27/28. The average amount of this extended β structure depended on the decapeptide variant, ranging from ≈5% (Dutch) to ∼32% (Iowa). These extended β structures corresponded to three distinct sporadic types of β-hairpin structures differing by the register of their dominant backbone HBs and labeled β_{28}, β_{29}, and β_{18}. The structure and dynamics of these β-hairpin structures are further examined in the following sections.

Role of Hydrogen Bonding and Hydrophobic Packing in Decapeptide Folding. The contact maps of Figures 1 and 2 and secondary structure (Figure II, Supporting Information) were derived by calculating time-averaged quantities using entire trajectories. These averages, however, do not accurately describe abundance nor frequencies of the different underlying structures, since the distributions from which these averages were derived were typically multimodal and the HB contacts did not occur with equal probability throughout each trajectory. To analyze the relative contribution of these structures, histograms of distances between pairs of C_α carbons, radius of gyration (R_g), and the SASA value for $S(4,8)$ for each of the four decapeptide variants were calculated and are shown in Figure 3.

dx.doi.org/10.1021/jp301619v | J. Phys. Chem. B 2012, 116, 6311−6325

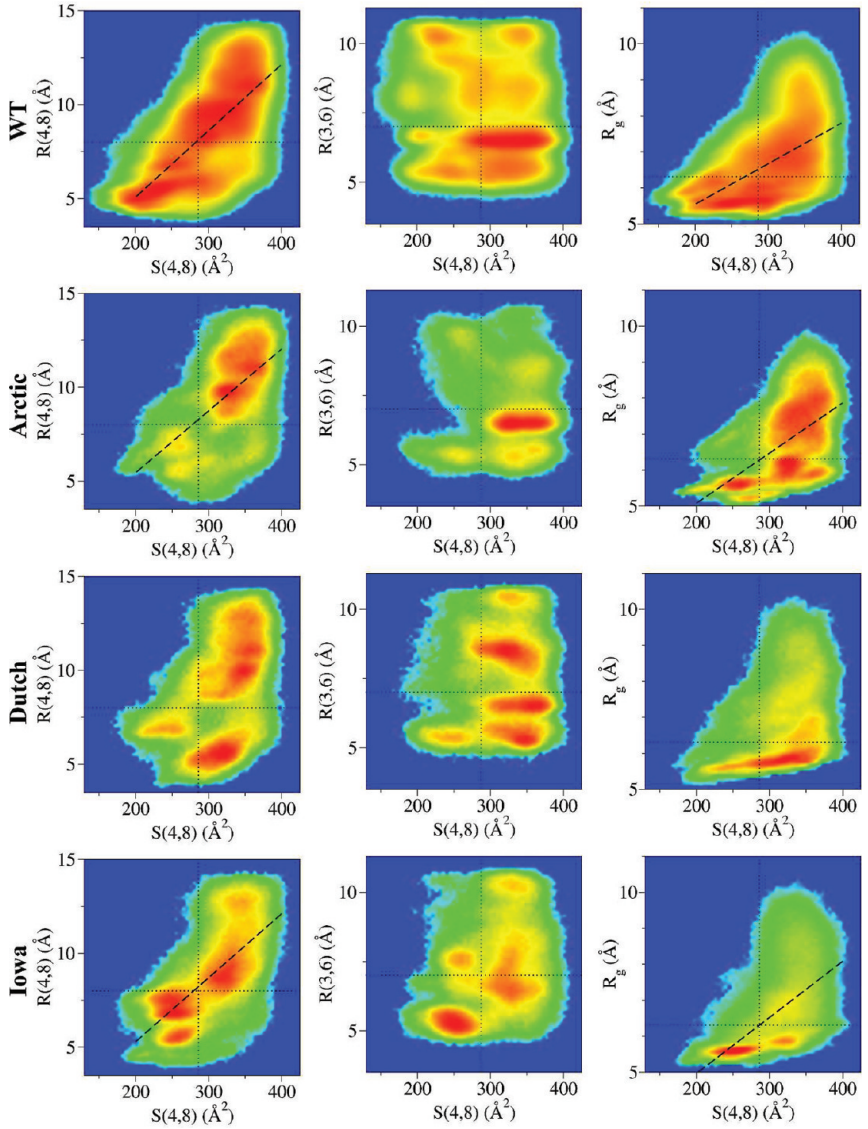

Figure 4. Two-dimensional maps corresponding to the normalized logarithm of the number of configurations $G[S,R]$ plotted according to their $R(4,8)$, $R(3,6)$, and R_g vs $S(4,8)$ values using the data from Figure 3. The rainbow colormap corresponds to the highest number of conformations (red) to zero conformations (blue). Thus, a point in a map with value $G[S,R]$ that is red indicates that that particular pair of $R(x,y)$ and $S(4,8)$ is populated by the maximum number of conformations. The dashed lines are linear regression fits to the data for only those data exhibiting significant correlations. For the WT $G[S(4,8),R(4,8)]$, the Pearson correlation coefficient, r, is $r = 0.71$, and for the $G[S(4,8),R_g]$, it is $r = 0.57$. For the Arctic $G[S(4,8),R(4,8)]$, the correlation coefficient is $r = 0.59$, and for the $G[S(4,8),R_g]$, it is $r = 0.55$. For the Iowa $G[S(4,8),R(4,8)]$, the correlation coefficient is $r = 0.68$, and for the $G[S(4,8),R_g]$, it is $r = 0.63$. The thin dotted vertical lines in the $S(4,8)$ axis are centered at 287 Å^2, while the horizontal lines at the $R(4,8)$, $R(3,6)$, and R_g axes are at 8, 7, and 6.3 Å, respectively.

For all four peptides, the $S(4,8)$ histograms exhibited a peak at ≈340 Å^2 (Figure 3, first column), which corresponded to the loop structure presented in the previous section. The other peaks at lower values of $S(4,8)$ (between 240 and 260 Å^2) in the Arctic, Iowa mutants, and to some extent also in the WT peptide, mostly corresponded to β-hairpin structures. The midpoint between the loop and these β-hairpin structures in these histograms was used to draw a dashed line at 287 Å^2 as a value that separates these distinct populations. Because Val24 and the n-butyl portion of Lys28 are hydrophobic, the low values of $S(4,8)$ indicated that the hydrophobic side chains were more effectively shielded from the solvent in the β_{28} and β_{29} hairpin structures than in the loop structures. However, the β_{18} hairpin structure in the Arctic had larger values of $S(4,8)$. The uncharacteristic high abundance of β-hairpin structures in the Iowa mutant, first observed in Figure 1, gave rise to a double peaked distribution.

The $R(3,6)$ distance histograms showed a bimodal distribution for $R(3,6) < 7$ Å in all decapeptides (Figure 3, second column). These two peaks were mostly populated by conformations with a high occurrence of HB pairs Asp23(O_δ)−Ser26(H) and Asp23(O_δ)−Ser26(H_γ) in the WT, Arctic, and Dutch mutants. These HBs were also among the dominant HBs (trajectory-wide) in these decapeptides (Table C, Supporting Information), and their propensity within and among these peptides corresponded to the relative heights of the $R(3,6)$ peaks. The high percentage of these HBs indicated that the $R(3,6)$ distance was the dominant structural feature in these three decapeptides, also consistent with Figure 1. In contrast, while these two peaks in the Iowa mutant were dominated by

dx.doi.org/10.1021/jp301619v | J. Phys. Chem. B 2012, 116, 6311−6325

structures exhibiting the HB pairs Asn23(H_δ)−Ser26(O) and Asn23(O_δ)−Ser26(H), these two HBs were not dominant when considering the whole trajectory (Table C, Supporting Information). Instead, the dominant HBs dictating the prevalent structure in the Iowa (Figure 1) came from the large population of β-hairpin conformations found at the $R(3,6) \approx 5.4$ Å peak (Figure 3, green line) sustained by the three dominant backbone HBs (listed in Table C, Supporting Information). A broader conclusion from the data of the four decapeptides is that, although HBs involving the Asp23−Ser26 amino acids dominated the $R(3,6)$ structure, the fact that there was a bimodal distribution ($R(3,6) \approx 5.4$ and 6.5 Å peaks) prevented the decapeptides from locking into a single conformation and allowed the loop to explore different, though related, structures. On the other side of the spectrum, the peak in the Dutch mutant at $R(3,6) \approx 8.5$ Å originated from the Asp23(O_δ)−Asn27(H) and Asp23(O_δ)−Asn27(H_δ) HBs. This peak was the most predominant in the Dutch mutant because of the higher combined percentage of these two HBs as compared with the other three decapeptides (Table C, Supporting Information).

The shapes of the $R(4,8)$ distance distributions (Figure 3, third column, black lines) suggested two regions of low and high $R(4,8)$ populations separated at $R(4,8) \approx 8$ Å. This separation was consistent with the compact structure, and thus low $R(4,8)$, of the β_{28} and β_{29} hairpins (green and blue lines) that were to the left of this separating line. In previous work,[41] this separating line was found at a smaller distance of 6.5 Å and was associated with hydrophobic events. However, because the $R(4,8)$ distances did not dominate the structure of the decapeptides (suggested by the lack of Val24−Lys28 contacts in Figure 1), hydrophobicity as indicated by the $S(4,8)$ played a reduced role in the present context. We note that the β_{18} conformations (orange lines in Figure 3) had increased values of $R(4,8)$, which when combined with their high values of $S(4,8)$ (e.g., in the Arctic, first column) suggested that these β_{18} hairpin structures might be more open than the β_{28} and β_{29} hairpins.

The histograms of the $R(2,8)$ and $R(3,8)$ distances showed the presence (or absence) of SBs between the negatively charged Glu22/Asp23 and positively charged Lys28 (Figure 3, fourth and fifth columns). These SBs were shown as sharp narrow peaks at a distance of ≈4 Å.[83] According to the charges of the Asp23 and Glu22, both SBs occurred in the WT peptide, whereas in the Arctic and Dutch mutant only the Asp23(O_δ)−Lys28(H_ζ) SB formed, and in the Iowa mutant only the Glu22(O_ε)−Lys28(H_ζ) SB was present. The area below the SB peaks in the $R(2,8)$ and $R(3,8)$ distance histograms was proportional to the number of SBs formed. This in turn reflected a low rate of SB formation, which was consistent with the percentage of SB formation (Table C, Supporting Information), suggesting a relatively small contribution of SBs to the decapeptide folding dynamics.

The R_g histograms (Figure 3, sixth column) for all of the decapeptide types included a peak at values of $R_g < 6.5$ Å consisting of compact loop conformations as well as all β-hairpin structures. The area A under the curve of each R_g distribution (up to $R_g = 6.5$ Å) indicated that the level of compactness was variant-specific. The Arctic mutant was, on average, the least compact ($A = 0.39$), followed by the WT peptide ($A = 0.49$), the Dutch mutant ($A = 0.52$), and the Iowa mutant ($A = 0.58$). The second peak in the Arctic mutant for $R_g > 6.5$ Å arose from structures that also had a large value of $S(4,8)$ (>287 Å^2), further examined below.

Next, possible correlations between key distances R ($R(4,8)$, $R(3,6)$, and R_g) from Figure 3 and the hydrophobic packing of Val24 and Lys28 side chains $S(4,8)$ were examined. Two-dimensional correlation maps were constructed in which for a given pair of values $[S(4,8),R]$ they: (i) counted the number of conformations simultaneously satisfying those two numbers and (ii) plotted $G[S(4,8),R]$, the normalized logarithm of this histogram (Figure 4). Data for $G[S(4,8),R(4,8)]$ shown in the first column of Figure 4 showed that $R(4,8)$ and $S(4,8)$ were positively correlated in the WT, Arctic, and Iowa variants, as indicated by their Pearson correlation coefficient $r = 0.71$, 0.59, and 0.68, respectively. The Dutch mutant, however, only showed a weak correlation with $r = 0.45$ where conformations with low $R(4,8)$ and high values for $S(4,8)$ (lower-right region) weakened the correlation. These results were preserved even when β-hairpins were excluded from the analysis (Figure III, Supporting Information). The regions with large $S(4,8)$ and $R(4,8)$ values (upper right) were the most populated in all peptides except in the Iowa mutant, which was characterized by a large population of β-hairpin structures with low $S(4,8)$ and $R(4,8)$ (lower-left region). This behavior was confirmed by calculating $G[S(4,8),R(4,8)]$ excluding all β-hairpin structures (Figure III, Supporting Information). In the second column of Figure 4, $G[S(4,8),R(3,6)]$ was examined to see whether the dominant Asp23−Ser26 HBs were correlated with hydrophobic packing events. No significant correlation was found, demonstrating that, regardless of the Asp23−Ser26 HB, most conformations had high $S(4,8)$ values (also in Figure III, Supporting Information). The exception was the Iowa mutant with the β-hairpin structures populating the low $S(4,8)$/low $R(3,6)$ value region (compared to Figure III, Supporting Information). An important feature is that the peaks in the distribution of $R(3,6)$ (Figure 3) were here segregated into unconnected "islands" with respect to $S(4,8)$, indicating distinct conformational subgroups differing not only by $S(4,8)$ but also by their predominant HBs. In the third column, $G[S(4,8),R_g]$ demonstrated a correlation between the compactness of the decapeptide structure and hydrophobic packing in the WT, Arctic, and Iowa variants with $r = 0.57$, 0.55, and 0.63, respectively. Again, in the Dutch mutant, this quantity showed only a weak correlation with $r = 0.35$. However, when excluding in the analysis all of the β-hairpin structures, only the WT preserved a significant correlation with $r = 0.54$ (Figure III, Supporting Information). This is in part because, when excluding the β-hairpin structures, the remaining conformations mostly corresponded to high values of $S(4,8)$ (first column of Figure 3, red curves) irrespective of compactness. Interestingly, the Dutch mutant with one of the most compact structures, even when excluding β-hairpin structures (R_g in Figure 3 black and red curves), had the weakest correlation between $S(4,8)$ and R_g, indicating that even when considering the most compact conformations, as exemplified in the Dutch variant, they would not necessarily result in hydrophobic packing. Overall, these maps suggested that the WT decapeptide sampled a larger R and $S(4,8)$ phase space than the mutants which were characterized by a more discrete set of preferred conformations in the form of highly populated phase space islands.

Clustering Analysis. To test whether decapeptide structures could be classified in terms of representative conformations regardless of their $R(4,8)$, $R(3,6)$, R_g, or

dx.doi.org/10.1021/jp301619v | J. Phys. Chem. B 2012, 116, 6311−6325

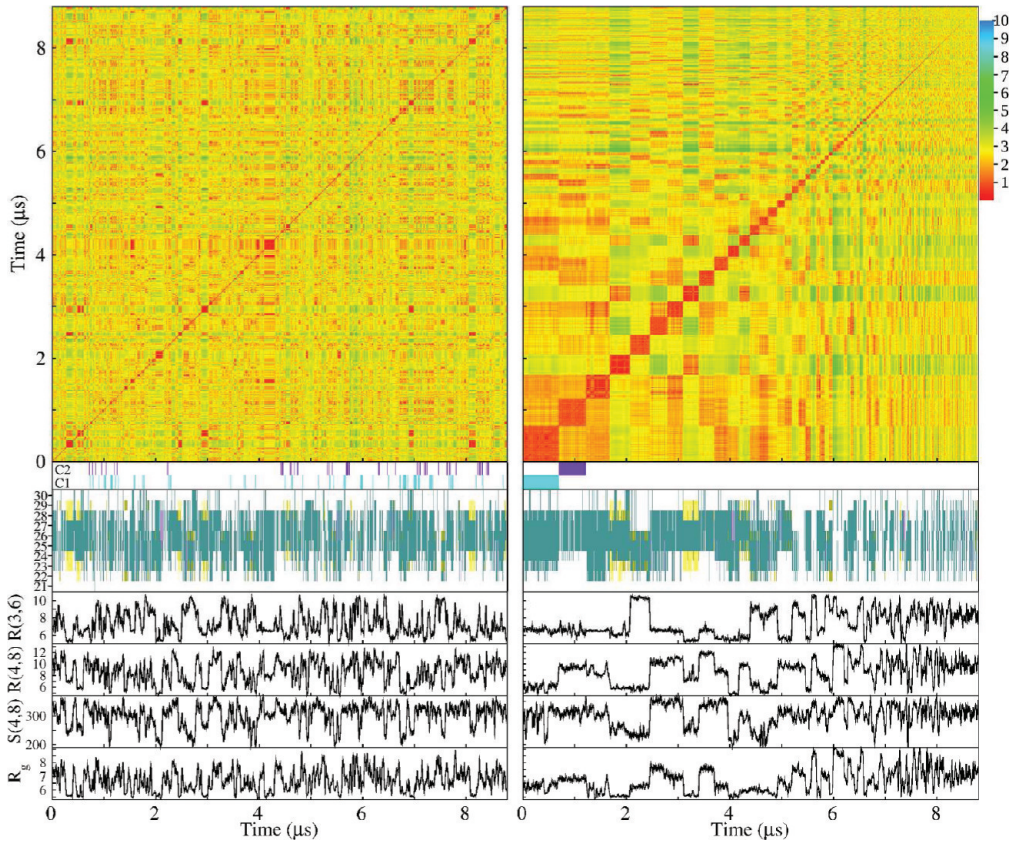

Figure 5. Clustering analysis for the WT trajectories. The analysis is presented in two ways: by concatenating all trajectories and analyzing them as a function of simulation time (left column) and by sorting the frames of all of the trajectories according to the cluster that each frame belongs to (right column). In each column, the top color matrix is the RMSD matrix indicating the RMSD distances between all pairs of trajectory frames. The cyan and purple horizontal bars (indicated by C1 and C2, respectively) mark those frames belonging to the most populated cluster (C1, cyan) and the second most populated (C2, purple). Below these bars, the secondary structure per amino acid for each frame is shown (colors correspond to turn - green, gold - bridge, yellow - extended β, and magenta - α helix). The four graphs below trace values for $R(3,6)$, $R(4,8)$, R_g (in Å), and $S(4,8)$ (in Å^2) for each trajectory frame.

$S(4,8)$ values, a clustering algorithm (described in the Methods section) was used. In Figure 5, the RMSD matrix of all concatenated trajectories of the WT is shown as a function of simulation time (upper left matrix). This matrix indicated, by using a colormap representation, the RMSD distance between any frame i (x-axis) and frame j (y-axis). Overall, this map indicated large variability of conformations with RMSD distances ranging from less than 1 Å to about 6 Å with small but significant clustering regions. To the right of this map, the same data was now sorted according to the cluster to which each time frame belonged (defined in the Methods section). The most populated cluster started at the (0,0) position followed by clusters of decreasing population size for increasing values of the x- and y-axes. The most populated cluster, denoted C1, comprised 7.7% of all conformations, followed by C2 and C3, with 5.9 and 5.4%, respectively. The significance of these percentage values as well as the definition of clusters and the correspondence of time frames to clusters is small, however, since all of these quantities were found to be strongly dependent on the choice of RMSD cutoff and not on intrinsic properties of the structures (Figures IV and V, Supporting Information). Nonetheless, under the current definition (RMSD cutoff = 1 Å), clusters were determined at every frame of the trajectories, identifying each frame as belonging to either C1 or C2 by using a cyan or purple bar below both RMSD matrices of Figure 5. The scattered distribution of frames in the unsorted matrix on the left belonging to C1 and C2 indicated that conformations belonging to C1 and C2 occurred throughout the length of the trajectories. Below these C1 and C2 colored bars, secondary structures as a function of simulation frame are presented. While in the unsorted trajectories secondary structure elements were uniformly distributed throughout the trajectories, in the sorted trajectories, there was clear indication of clustering corresponding to C1, C2, C3, etc. The sorted trajectories indicated that, for structures belonging to C1, C2, and C3, amino acids in the central part of the decapeptide exhibited similar turn structures. In contrast, cluster C4 corresponded to β-hairpin conformations. In the four lower graphs in Figure 5, the quantities $R(3,6)$, $R(4,8)$, $S(4,8)$, and R_g again assumed a wide range of values in the unsorted trajectories unlike in the sorted frame sequences where they exhibited regions of constant values that corresponded to each cluster. Importantly, whereas $R(3,6)$ showed a relatively constant value for clusters C1, C2, and C3 in the sorted trajectories (at about 6.5 Å), the other quantities varied radically from cluster to cluster. This result indicated that, while there was a commonality in the values of $R(3,6)$ among the predominant clusters, these clusters were nonetheless distinct from each other in other structural aspects, thus indicating the absence of a dominating single representative conformation.

dx.doi.org/10.1021/jp301619v | J. Phys. Chem. B 2012, 116, 6311−6325

Structural Characteristics of the β-Hairpin Conformations. To study in more detail the extended β structures found in the average secondary structure analysis (Figure II, Supporting Information), the time evolution of the secondary structure was examined. At least three distinct sporadic types of β-hairpin structures were identified (Figure VI, Supporting Information), the β_{28}, β_{29}, and β_{18} discussed above, that differed by the register in which pairs of amino acids formed hydrogen bonds. The different registers are shown in Figure 6. For the β_{28} type, the dominant backbone HBs were between Glu22−Lys28, Ala21−Ala30, and Val24−Ser26 (see Table 1). For the β_{29} type, the dominant backbone HBs were between Glu22−Gly29 and Val24−Asn27. For the β_{18} type, the dominant HB was between Ala21−Lys28. A complete list of the HB propensities within the three β-hairpin conformations is given in Table 1. Comparison between HB pair propensities (Table C, Supporting Information) and HB propensities for particular β-hairpin conformations (Table 1) showed that the loop and β-hairpin conformations fundamentally differed. Whereas the β-hairpin structures were associated with the backbone−backbone HB formation, the loop conformations did not have any appreciable backbone−backbone HBs but rather formed HBs between the charged side chain group of Asp23(O_δ) and either backbone atoms or other side chain groups.

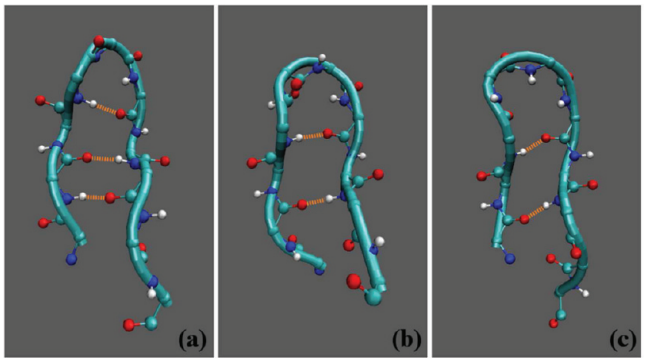

Figure 6. Snapshots of β-hairpin conformations for the WT showing some of the dominant backbone HBs (orange dashed lines) that define each different register. These HBs are (from bottom to top): (a) β_{28} between Glu22(H)−Lys28(O), Glu22(O)−Lys28(H), and Val24-(H)−Ser26(O); (b) β_{29} between Glu22(O)−Gly29(H) and Val24-(H)−Asn27(O); and (c) β_{18} between Ala21(H)−Lys28(O) and Ala21(O)−Lys28(H). Conformations show the N termini on the left end of the decapeptide. Only backbone atoms are displayed.

Because of the specific register of the three β-hairpin types, the Val24 and Lys28 side chains were found to be located at fixed positions relative to each other yet not necessarily in proximity. Specifically, in the β_{28} type, the Val24 and Lys28 side chains were on the same side of the hairpin and adjacent to each other (Figure VII, top, Supporting Information). However, in the β_{29} type, they occupied opposite sides of the hairpin (Figure VII, middle, Supporting Information). In the β_{18} type, they were on the same side, but the side chain of Val24 was within the turn region pointing away from the Lys28 side chain (Figure VII, bottom, Supporting Information). These data indicated that the quantity $S(4,8)$ would not be an appropriate metric for hydrophobic events in the β-hairpins, as low values would not necessarily indicate proximity and hydrophobic contact between Val24 and Lys28 as had been the case for the loop. An alternate measure, the SASA of the whole decapeptide, is discussed below.

Different β-hairpin type structures occurred at different proportions for each decapeptide variant (Table D, Supporting Information). The particularly high percentages of β_{28} and β_{29} in the Iowa mutant were already evident in the strong diagonal contacts in Figure 1, a clear signature of β-hairpin structures. Taken as a whole, these results demonstrated that the absence of charge at position 22 decreased the β_{29} occurrence, whereas the absence of charge at position 23 increased β_{28} and β_{29} occurrences. The β_{18} occurrence percentage increased for the Arctic mutant. However, of the three β-hairpins, the β_{18} was the most insensitive to mutations.

Degree of Stability of the β-Hairpin Conformations. A simple observation of the time evolution of the β-hairpin structures revealed that these structures would form and unfold, although in a few cases they would remain folded for the duration of the trajectory. Numerous studies[38−43,51−53,63,84−86] (also text and Figure VIII in the Supporting Information), however, have shown that this decapeptide does not have stable conformations. Thus, the behavior observed here can only be attributed to metastable β-hairpin structures with low occurrence probabilities, manifested in our current dynamical trajectories as short-lived conformations.

Examination of the time evolution of the secondary structure suggested that the β-hairpins had characteristic *formation times* and *lifetimes* (the typical time that a β-hairpin structure existed before unfolding or converting into another β-hairpin type) that may be sensitive to mutations at positions 22 and 23. Here, only the lifetime of each β-hairpin structure was examined as a measure of the degree of stability. Visual inspection of the fluctuations in the extended structure (Figure VI, Supporting Information) initially suggested that the β_{28} type was more stable than the β_{29} type, followed by the least stable β_{18} type, consistent with the number of dominant backbone HBs of each β hairpin type, namely, 3, 2, and 1 (see Table 1).

To measure lifetimes, independent trajectories labeled i were started from preformed β-hairpins and their breaking times τ_i were measured. Lifetimes were then calculated by an exponential fit to the set $\{\tau_i\}$, as described in the Methods section. Specifically, τ_i were obtained by examining the secondary structure as a function of simulation time. The times at which the extended β conformations disappeared were then recorded as τ_i. A secondary criterion for τ_i was obtained by examining, in a similar way, the RMSD between the starting conformation (β-hairpin at $t = 0$) and all conformations at later times. The times at which the RMSD rapidly increased were recorded as τ_i. The respective τ_i obtained through these two methods typically coincided (Figure IX, Supporting Information).

In Figure 7, results for all $\{\tau_i\}$ from 10 independent trajectories per decapeptide variant for each of the β-hairpin types are plotted. The number at the top of each graph is the calculated lifetime for that particular β-hairpin structure (see the Methods section for details). Open symbols indicate a trajectory in which the β-hairpin did not break within the maximal observation time of 400 ns. For the β_{28} in the Dutch mutant, a lifetime could not be calculated due to the high number of unbroken β-hairpins but was considered to have a lower bound of no less than 500 ns when compared with the β_{28} and β_{29} in the Iowa. Overall, the breaking times were typically higher for β_{28} and lower for β_{29} and β_{18} in all four decapeptide variants. In the WT peptide, one β_{18} trajectory may have biased the β_{18} lifetime to a value greater than the one for the β_{29} trajectories. On the basis of the lifetimes of the

dx.doi.org/10.1021/jp301619v | J. Phys. Chem. B 2012, 116, 6311−6325

Table 1. Table of HB Percentages for All β-Hairpin Types and Decapeptide Variants[a]

	β_{28}				β_{29}				β_{18}			
hydrogen bond (%)	WT	Arctic	Dutch	Iowa	WT	Arctic	Dutch	Iowa	WT	Arctic	Dutch	Iowa
					SB							
Glu22(O_ε)−Lys28(H_ζ)												
Asp23(O_δ)−Lys28(H_ζ)					**27.9**	**23.9**	**22.9**		12.7	2.9	16.1	
					Charged-SC							
Glu22(O_ε)−Asp23(H)	3.9			4.1	4.3			9.0				
Glu22(O_ε)−Asn27(H_δ)									**14.9**		2.8	**17.1**
Asp23(O_δ)−Val24(H)									1.4		1.5	
Asp23(O_δ)−Gly25(H)	9.5	12.6	8.8	5.0	2.8	3.2	2.8	2.2	4.8	**9.9**	1.5	
Asp23(O_δ)−Ser26(H)						3.3	6.3		5.0	2.2	1.1	
Asp23(O_δ)−Ser26(H_γ)									5.7	5.9	1.8	
Gly25(O)−Lys28(H_ζ)						1.0						
Ser26(O_γ)−Lys28(H_ζ)										1.7		
Ala30(O)−Lys28(H_ζ)		5.1								1.2		2.5
					Backbone-Backbone							
Ala21(O)−Lys28(H)									**21.6**	**22.9**	**24.1**	**17.3**
Glu22(O)−Lys28(H)	**19.3**	**20.9**	**21.2**	**19.4**								
Glu22(O)−Gly29(H)					**29.5**	**24.1**	**28.2**	**32.9**				
Asp23(O)−Ser26(H)										5.2		
Ser26(O)−Asp23(H)									2.6	9.3	**19.4**	2.5
Ser26(O)−Val24(H)	**20.3**	**20.6**	**19.9**	**24.8**								
Asn27(O)−Val24(H)					**13.9**	**20.2**	**18.1**	**29.8**				
Lys28(O)−Ala21(H)		3.0							**23.4**	**9.8**	**19.5**	**27.5**
Lys28(O)−Glu22(H)	16.5	13.4	19.2	15.3								
Gly29(O)−Ala21(H)									1.5	8.7		3.4
Gly29(O)−Glu22(H)					9.9	8.8	11.6	**9.1**				
Ala30(O)−Ala21(H)	**24.8**	**20.2**	**25.9**	**27.8**	2.5	9.4	1.8	2.9	2.0	8.8	1.5	10.1
Ala30(O)−Glu22(H)					2.3	1.3		2.7				
					SC-Backbone							
Gly25(O)−Asn23(H_δ)								2.8				
Gly25(O)−Ser26(H_γ)							1.2					
Ser26(O)−Asn23(H_δ)												10.8
Ser26(O_γ)−Asn23(H_δ)												1.0
Asn27(O_δ)−Ala21(H)										3.3	1.7	2.1
Asn27(O_δ)−Gly29(H)										3.6		1.1
Lys28(O)−Asn27(H_δ)					3.7	1.5		4.8				
Ala30(O)−Gln22(H_ε)							3.2					

[a]This table was compiled using data gathered from the pre-formed β-hairpin trajectories. Only HBs with percentages greater than 1% are listed. The three most prevalent HB bonds are indicated in bold.

dominant β_{28} and β_{29} hairpins, these results separated the four decapeptide variants into two groups: (i) the WT and Arctic mutant, with lifetimes below 200 ns, and (ii) the Dutch and Iowa mutants, with lifetimes above 200 ns and as high as 500 ns. For comparison, a similar analysis performed using the C1 and C2 clusters in the WT trajectories (using the data from the cyan and purple bars of Figure 5) yielded a loop lifetime of 15.88 ± 0.11 and 13.60 ± 0.10 ns for the C1 and C2 loop conformations, respectively (Figure X, Supporting Information). These loop lifetimes were an order of magnitude smaller than any of the WT β-hairpin structures.

The distinct lifetimes of the three β-hairpin structures could be associated with $S(2-4,6-8)$, the combined SASA of the decapeptide excluding the glycines and the two terminal alanines. Specifically, low $S(2-4,6-8)$ values could potentially indicate a more stable structure with more hydrophobic contacts. To evaluate this possibility, average values for $S(2-4,6-8)$ were calculated for each of the decapeptide and β-hairpin types (Table E, Supporting Information) by calculating the average $S_i(2-4,6-8)$ per trajectory (10 per β hairpin type), averaging over all S_i to obtain $\langle S(2-4,6-8)\rangle$, and normalizing this average by the values of each stretched decapeptide variant, $S_{ext}(2-4,6-8)$. This normalization was necessary because the range of $S(2-4,6-8)$ values was variant-dependent (e.g., Arctic had a smaller range of $S(2-4,6-8)$ values than the WT because of the [Glu22Gly] substitution). $S_{ext}(2-4,6-8)$ for each variant was obtained by using fully stretched decapeptides. The total times over which each average was determined are listed in Table F, Supporting Information. To test whether the lifetimes were correlated with $S(2-4,6-8)$, the dependence of lifetimes vs $S(2-4,6-8)$ was plotted (Figure 8). The lifetime of the β_{28} in the Dutch mutant was set here to 500 ns. The data in Figure 8 demonstrated that the β_{28} (black) and β_{18} (green) lifetimes significantly decreased with increasing $S(2-4,6-8)$; thus, a higher exposure to solvent decreased their lifetimes. However, this correlation was not evident for the β_{29} type. In the following, the nature of the lifetimes of each of the β_{28}, β_{29}, and β_{18} hairpins is discussed.

For the first case, having established that for the β_{28} hairpin type the WT and Arctic decapeptides had shorter lifetimes

dx.doi.org/10.1021/jp301619v | J. Phys. Chem. B 2012, 116, 6311−6325

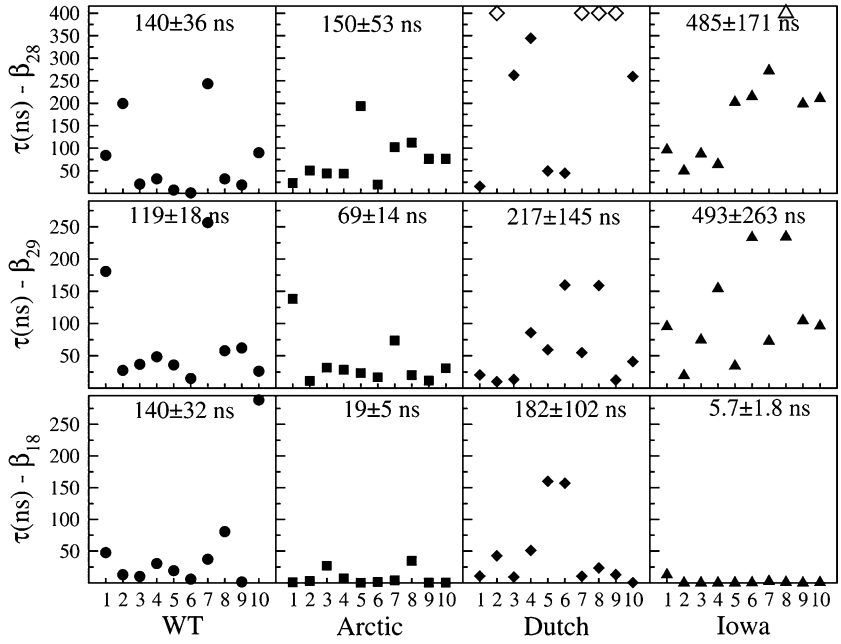

Figure 7. Breaking times τ_i obtained for each of 10 trajectories per β-hairpin and decapeptide type. The number at the top of each graph is the average lifetime and standard deviation obtained by fitting an exponential distribution to the data (see the Methods section).

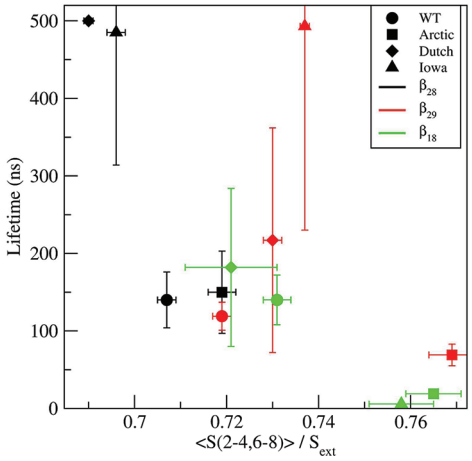

Figure 8. Dependence of the β-hairpin lifetimes on the normalized total SASA of the decapeptide excluding the glycines and two terminal alanines, $\langle S(2{-}4,6{-}8)\rangle/S_{ext}$. The symbols correspond to WT - circle; Arctic - square; Dutch - diamond; and Iowa - triangle. The different β-hairpins are denoted by the color of the symbol, where β_{28} is black, β_{29} is red, and β_{18} is green. Error bars correspond to the standard error of the mean.

(~150 ns) than the Iowa (485 ns) and Dutch (≥500 ns) because their side chains were more exposed to the solvent (Figure 8), specific amino acids were probed to examine their role in reducing the solvent exposure. In Figure XI in the Supporting Information, contributions from different SASA combinations of amino acids are plotted for all four decapeptide variants. For the β_{28} type, minima in $S(2{-}4,6{-}8)$ were caused by decreased $S(2,4,8)$ (in the Dutch mutant) or decreased $S(3,7)$ and $S(3,6)$ (in the Iowa mutant). By examining representative structures (using the cluster analysis described in the Methods section but now only using β-hairpin structures), it was observed that, whereas the side chains of Val24 and Lys28 were on the same side of the hairpin loop (Figure VII, Supporting Information), the Gln22 side chain in the Dutch mutant closely packed with the Val24 and Lys28 side chains, thus lowering the effective $S(2,4,8)$ (Figure XII, Supporting Information). In contrast, in the WT and Iowa mutant, the Glu22 side chain was solvated. In the Arctic mutant, this packing was also missing, as the Gly22 lacked a side chain. This observed Gln22−Val24−Lys28 packing in the Dutch mutant also enhanced the lifetime of the structure by reducing the fluctutations between the side chains of Val24 and Lys28, which was consistent with a narrower distribution of the dot product D between the vectorial directions of the Val24 and Lys28 side chains (Figure XIII, Supporting Information). By examining a representative structure of the Iowa β_{28} type structure, it was observed that the dip in $S(3,7)$ (Figure XI, top, Supporting Information) was caused by the Asn23−Asn27 hydrophobic packing (Figure XIV, Supporting Information). The additional reduction in the value of $S(3,6)$ for the Iowa mutant (Figure XI, top, Supporting Information) did not independently contribute to a longer lifetime, since the Asp23 and Ser26 side chains were on opposite sides of the β_{28} hairpin but rather reflected the decrease in the $R(3,7)$ distance resulting from the Asn23−Asn27 hydrophobic packing discussed above.

Additional contributions to the increased lifetime of the Dutch and Iowa β_{28} hairpin type structures came from their backbone HBs. In Figure 9, the lifetimes of β-hairpins are plotted as a function of the "effective HB percentage". These effective HB percentages were derived from Table 1 by adding up all in-register backbone HBs (middle section of that table) while subtracting the percentage of "competing" HBs. Specifically, for the β_{28} type, the effective HB percentages were obtained by adding up all Glu22−Lys28, Val24−Ser26, and Ala21−Ala30 contributions while subtracting the contribution from Lys28(O)−Ala21(H) that competed with the formation of the Lys28(O)−Glu22(H). For the β_{29} type, all of the backbone HBs were included except Ala30(O)−Glu22(H), which was subtracted due to the competition with Gly29(O)−Glu22(H). Similarly, for the β_{18} type, the contributions from Gly29(O)−Ala21(H) and Ala30(O)−Ala21(H) HBs were subtracted because they competed with formation of the

dx.doi.org/10.1021/jp301619v | J. Phys. Chem. B 2012, 116, 6311−6325

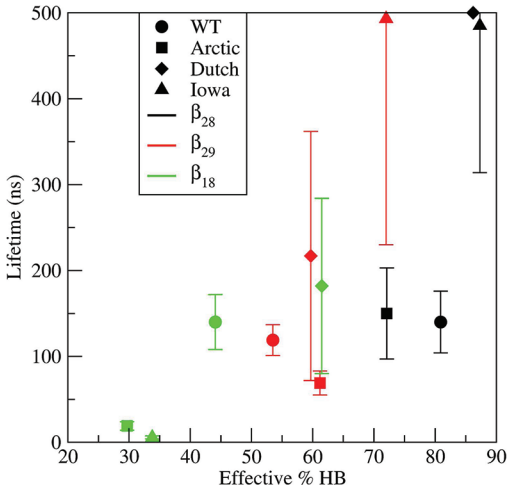

Figure 9. Dependence of β-hairpin lifetimes on the effective backbone hydrogen bonding propensity. The symbols correspond to WT - circle; Arctic - square; Dutch - diamond; and Iowa - triangle. The different β-hairpins are denoted by the color of the symbol, where β_{28} is black, β_{29} is red, and β_{18} is green.

Lys28(O)−Ala21(H) HB. In Figure 9, the β_{28} in the Dutch and Iowa mutants had larger effective HB percentages than the WT and Arctic. These results demonstrated that both reduced SASA and an increase in backbone HBs contributed to longer lifetimes of the β_{28} hairpin in the Dutch and Iowa mutants.

For the case of the β_{29} hairpins, the lifetimes of the Arctic (<70 ns) and Iowa (≈500 ns) mutants were respectively lower and higher than the lifetimes of the WT and Dutch mutants (100−200 ns). In terms of SASA, the small lifetime of the β_{29} in the Arctic mutant corresponded to an increased value of S(2−4,6−8), indicating an increased exposure to the solvent relative to the other variants (Figure XI, middle, Supporting Information). On the other hand, the long lifetime in the β_{29} Iowa hairpin could not be attributed to a reduced overall SASA, as none of the $S(x,y)$ values (Figure XI, Supporting Information) was significantly smaller than those for the WT peptide. Also, examination of representative structures in the Iowa mutant did not reveal any other hydrophobic contacts that could lengthen the lifetime of the hairpin. The long lifetime of the Iowa β_{29} type was most likely caused by the backbone HBs, consistent with the highest value of the effective HB percentage (Figure 9). Interestingly, this higher effective HB percentage in the Iowa occurred even in the absence of the Asp23−Lys28 SB (Table 1), suggesting that the absence of this SB was compensated by an increase in the backbone HBs, resulting in a longer lifetime.

The lifetimes of the β_{18} hairpins for the WT and Dutch mutants had values between 100 and 200 ns, whereas for the Arctic and Iowa mutants these lifetimes were below 20 ns (Figure 7). In the graph of the lifetime versus S(2−4,6−8) (Figure 8), the lifetime of the β_{18} hairpin decreased with increasing SASA. Thus, the Arctic and Iowa mutants with considerably larger SASA values had on average correspondingly smaller β_{18} hairpin lifetimes. An additional destabilizing factor was found when examining the effective HB percentages vs lifetimes (Figure 9), in which the Arctic and Iowa mutants with the shortest β_{18} hairpin lifetimes had the smallest effective HB percentages. This low value of the effective HB percentage was a result of the large number of HBs incompatible with the β_{18} hairpin, such as the Gly29/Ala30−Ala21 HBs (Table 1).

In sum, increased lifetimes in the β_{28} hairpin were a result of strong hydrophobic contacts involving Gln22, Val24, and Lys28 side chains in the Dutch mutant and the weaker but relevant Asn23−Asn27 contact in the Iowa mutant. For the case of the β_{29} hairpin lifetimes, the number of backbone HBs was the most influential factor where in particular the increased lifetime in the Iowa mutant was consistent with an increased number of backbone HBs originating from the absence of the Asp23−Lys28 SB. Lastly, the β_{18} hairpin lifetimes were also affected by hydrophobicity and by the competing HBs in the Iowa and Arctic mutants that destabilized the hairpin, whereas, in the WT and Dutch mutants, the Asp23−Lys28 SB helped sustain the β_{18} hairpin structure.

DISCUSSION

Constant temperature MD simulations of the Aβ_{21-30} decapeptide and its Arctic, Dutch, and Iowa mutants in explicit water revealed three long-lived metastable β-hairpin structures (β_{28}, β_{29}, and β_{18}) that differed in registers and number of backbone−backbone HBs and appeared with different propensities in all four variants. Their lifetimes were also strongly variant-dependent. Results from the WT suggested that β-hairpin lifetimes may be an order of magnitude larger than lifetimes of loop conformations. Hydrophobic packing of side chains resulted in increased lifetime of the β_{28} in the Dutch (Gln22−Val24−Lys28) and Iowa (Asn23−Asn27) mutants, whereas in the β_{29} hairpins lifetimes were mostly influenced by backbone−backbone HBs. Overall, formation of SBs did not play a major role in β-hairpin lifetimes. However, the lack of a Asp23−Lys28 SB in the Iowa increased the number of backbone HBs, resulting in an increased lifetime. Finally, the short lifetimes found in the β_{18} hairpin were attributed to the competition among the backbone HBs of different registers.

These β-hairpin structures comprised ∼5−12% of all structures in the WT, Arctic, and Dutch mutant and up to ∼32% in the Iowa mutant, with uninterrupted structural persistence from tens to hundreds of nanoseconds. Nonetheless, the overwhelming total population of coil and loop structures in any given trajectory suggested that the free energy of the β-hairpins, with comparatively lower solvent exposure from the tightly packed side chains, increased intrapeptide contacts, and lower potential energy due to backbone−backbone HBs, could not compete with that from the coil and loop structures which benefited from the much larger entropic contribution of these structurally looser structures. Because of the majority of loop conformations, when considering whole-trajectory averages, these β-hairpins did not dominate the predominant structural characteristics. These predominant structural characteristics for most decapeptide variants showed instead a strong Asp23−Ser26 interaction involving at least two HBs, a loop structure with a turn comprising amino acids 23−27, and unstructured N- and C-termini, previously observed in other studies.[38−43,51,52,85] A low rate of SB formation was found (also seen in ref 86), suggesting a relatively small contribution of SBs to the decapeptide conformational dynamics. Detailed whole-trajectory analysis of HBs also revealed that the Iowa mutant displayed a distinct HB network as compared with the WT, indicating that the absence of charge at position 23 profoundly changed the dynamics of HB formation, whereas the absence of charge at position 22 left the HB network intact, also consistent with previous studies.[52,53] In contrast to previous work, clustering analysis including all conformations failed to show a dominating loop

dx.doi.org/10.1021/jp301619v | J. Phys. Chem. B 2012, 116, 6311−6325

representative structure in the WT (largest cluster <8% of the total trajectory) but rather a multitude of clusters. While these clusters of loop structures shared structural properties such as the $R(3,6)$ distance and common HBs emanating from the Asp23(O_δ), they were structurally different from each other and displayed short lifetimes with a high rate of interconversion between them.

The existence and long lifetimes of the β-hairpin structures found here is not ubiquitous in all computational studies. Previous REMD studies on Aβ_{21-30} and its mutants have been characterized by a paucity or absence of β-hairpin structures.[39,52,53,85] On the other hand, a full-length Aβ_{1-40} and Aβ_{1-42} REMD study reported a β-turn formation in the Aβ_{1-40}.[57] In addition, constant temperature MD of the full-length Aβ have shown evidence of a β-hairpin in the 21−30 region,[87] while discrete MD studies using a coarse-grained peptide model also found evidence for a β-hairpin structure in the decapeptide region within Aβ_{1-40}, Aβ_{1-42}, and their Arctic mutants.[60,61] A possible explanation for this discrepancy could be that, whereas β-hairpin structures are metastable states with low occurrence probability, the mechanisms by which they fold are more readily accessible in simulations that examine dynamics and time evolution of the Aβ. Another possibility is that other mechanisms intrinsic to the formation of the β-hairpins presented here are at play, such as possible anti-Arrhenius behavior found in the folding rates of β-hairpins in some proteins[88−90] that may need a special treatment when examined by REMD.[91,92] Other reasons could also include that simulation times used in REMD may have to be greater than the folding times of the β-hairpins studied here[93] or that REMD might not show the folding.[94]

Our data, and that of others, demonstrate that the majority loop conformation observed in all four decapeptide variants was not static but rather comprised many short-lived conformations that interconvert with time.[52] This result raises the question of how could such a dynamic loop population nucleate the folding of the full-length Aβ. The present work elucidates the dynamics of three metastable β-hairpin structures that could play a critical role in nucleating full-length Aβ folding and affect the assembly pathway. The stability and structure of intermediates have been shown to affect protein folding, misfolding, and amyloid formation.[67] The β-hairpins studied here represent metastable states that could, in principle, nucleate the fold of the full-length Aβ by initially forming within the 21−30 region and then propagating into a β structure comprising the 17−22 and 28−37 regions.[54,95] This process is consistent with an experimental study that stabilized a β-hairpin of Aβ_{1-40} in the decapeptide region by binding Aβ_{1-40} to the affibody ZAβ3.[96] This view is consistent also with studies that showed that a preformed lactam bridge in the decapeptide region of Aβ_{1-40} strongly enhanced the rate of fibrilization[65,97] and produced toxic oligomeric species.[66] In our proposed scenario, the nucleation of a full-length Aβ fold by formation of the β-hairpin in the 21−30 region may be then followed by a subsequent loss of this same β-hairpin structure to become a turn, consistent with other full-length Aβ simulations.[58]

The results presented in this study suggest that longer β-hairpin lifetimes correlate with the degree of aggregation. Clinically, Dutch mutation carriers suffer from recurrent strokes and exhibit diffuse plaques and massive cerebral amyloid angiopathy (CAA).[49] *In vitro* studies have demonstrated that Dutch Aβ polymerizes into protofibrils and then into fibrils significantly faster than does WT Aβ.[98] This may be reflected *in vivo* by accelerated aggregation and deposition on the surface of endothelial cells and cerebrovasculature smooth muscle cells, causing damage.[99] Our results showed that the Dutch exhibited significantly longer β-hairpin lifetimes than the WT, Arctic, and Iowa mutants.

Similarly, the Iowa mutant had the largest propensity to form β-hairpins. These β-hairpins were also shown to have a substantially longer lifetime compared to the WT and Arctic mutants (but shorter than the Dutch). Clinically, the Iowa mutant also exhibits diffuse plaques with massive CAA similar to the Dutch but rarely exhibits strokes or hemorrhage,[45,100] in contrast to the Dutch. It is plausible that the relatively large β-hairpin lifetimes (similarly to the Dutch) and the large propensity to form β-hairpins (different from the Dutch) in the Iowa mutant combine to produce the massive CAA but result in an assembly pathway distinct from that of the Dutch mutant.

While there are differences between the Dutch and Iowa, there are also similarities. The β-hairpin lifetime results presented above separated the decapeptides into two classes: the WT and Arctic, with lifetimes less than 200 ns, and the Dutch and Iowa, with lifetimes of at least 500 ns. Experiments also show this separation. The Dutch and Iowa mutations are clinically, pathologically, and *in vitro* very similar,[45,101] leading to symptoms and pathologies distinct from AD.[102] On the other hand, the Arctic mutation exhibits clinical and pathological features typical of AD such as compact plaques, a fibrillization rate similar to the WT, and progressive dementia without stroke or hemorrhage. Also, the Arctic mutation does not exhibit the severe CAA that characterizes other mutations in the Aβ region of APP such as the Dutch and the Iowa mutations.[46,47]

Nonetheless, the Arctic stands out on its own. While it produces clinical and neuropathological features indistinguishable from those of late-onset sporadic AD, it produces them prematurely.[46,47] *In vitro* studies suggested that increased generation of intermediate protofibrillar Aβ assemblies formed early during fibrillogenesis may play a role in the pathology compared to WT.[46,103,104] It is possible that the differences observed in this paper in the Arctic mutant regarding its intramolecular HB (enhanced over the other decapeptide types) play a role in these differences.

In summary, constant temperature all-atom molecular dynamics simulations to study the dynamics of monomeric Aβ_{21-30} in explicit water and its Dutch [Glu22Gln], Arctic [Glu22Gly], and Iowa [Asp23Asn] isoforms revealed a majority of loop conformers predominantly exhibiting a hydrogen bond network involving the Asp23 and Ser26 amino acids. A minority but important population of conformers forming metastable β-hairpin structures were also observed. Measurements of the lifetimes of the dominant β-hairpins indicated that the Dutch mutant had the longest β-hairpin lifetime (greater than 500 ns), closely followed by the Iowa mutant (≈500 ns), while the Aβ_{21-30} and the Arctic mutant had significantly lower lifetimes (≈200 ns). The connection with clinical and pathological data suggests that the lifetimes and β-hairpin formation propensity may correlate with the degree of aggregation. Stabilizing or preventing intermediates prone to amyloid formation may prevent toxic assembly.[67] Experimental studies have shown that targeting the central region of the Aβ using antibodies and fragments inhibited Aβ aggregation.[105−107] The results of our study suggest that targeting the stability of

the metastable β-hairpin structures studied here could, in principle, be of therapeutic utility.

■ ASSOCIATED CONTENT

Supporting Information

Detailed simulation results. This material is available free of charge via the Internet at http://pubs.acs.org.

■ AUTHOR INFORMATION

Corresponding Author

*E-mail: ccruz@drexel.edu. Phone: (215) 895-2739. Fax: (215) 895-5934.

Notes

The authors declare no competing financial interest.

■ ACKNOWLEDGMENTS

Financial support was provided by National Institutes of Health grants AG023661, NS038328, and AG027818, the Jim Easton Consortium for Alzheimer's Drug Discovery and Biomarkers at UCLA, and the California Alzheimer's Disease Research Fund grant no. 07-65806. Computational time was provided in part by TeraGrid computational resources grant TG-MCB110142.

■ ABBREVIATIONS

Aβ, amyloid β-protein; AD, Alzheimer's disease; HB, hydrogen bond; MD, molecular dynamics; SASA, solvent accessible surface area; SB, salt bridge

■ REFERENCES

(1) Hardy, J.; Selkoe, D. J. *Science* **2002**, *297*, 353.
(2) Hardy, J.; Allsop, D. *Trends Pharmacol. Sci.* **1991**, *12*, 383.
(3) Pike, C. J.; Walencewicz, A. J.; Glabe, C. G.; Cotman, C. W. *Brain Res.* **1991**, *563*, 311.
(4) Hardy, J. A.; Higgins, G. A. *Science* **1992**, *256*, 184.
(5) Kirkitadze, M. D.; Bitan, G.; Teplow, D. B. *J. Neurosci. Res.* **2002**, *69*, 567.
(6) Lambert, M. P.; Barlow, A. K.; Chromy, B. A.; Edwards, C.; Freed, R.; Liosatos, M.; Morgan, T. E.; Rozovsky, I.; Trommer, B.; Viola, K. L.; Wals, P.; Zhang, C.; Finch, C. E.; Krafft, G. A.; Klein, W. L. *Proc. Natl. Acad. Sci. U.S.A.* **1998**, *95*, 6448.
(7) Walsh, D. M.; Klyubin, I.; Shankar, G. M.; Townsend, M.; Fadeeva, J. V.; Betts, V.; Podlisny, M. B.; Cleary, J. P.; Ashe, K. H.; Rowan, M. J.; Selkoe, D. J. *Biochem. Soc. Trans.* **2005**, *33*, 1087.
(8) Klein, W. L.; Stine, W. B.; Teplow, D. B. *Neurobiol. Aging* **2004**, *25*, 569.
(9) Teplow, D. B.; Lazo, N. D.; Bitan, G.; Bernstein, S.; Wyttenbach, T.; Bowers, M. T.; Baumketner, A.; Shea, J. E.; Urbanc, B.; Cruz, L.; Borreguero, J.; Stanley, H. E. *Acc. Chem. Res.* **2006**, *39*, 635.
(10) Haass, C.; Selkoe, D. J. *Nat. Rev. Mol. Cell Biol.* **2007**, *8*, 101.
(11) Roychaudhuri, R.; Yang, M.; Hoshi, M. M.; Teplow, D. B. *J. Biol. Chem.* **2009**, *284*, 4749.
(12) Walsh, D. M.; Selkoe, D. J. *J. Neurochem.* **2007**, *101*, 1172.
(13) Lesne, S.; Koh, M. T.; Kotilinek, L.; Kayed, R.; Glabe, C. G.; Yang, A.; Gallagher, M.; Ashe, K. H. *Nature* **2006**, *440*, 352.
(14) Urbanc, B.; Cruz, L.; Teplow, D.; Stanley, H. E. *Curr. Alzheimer Res.* **2006**, *3*, 493.
(15) Fink, A. L. *Curr. Opin. Struct. Biol.* **2005**, *15*, 35.
(16) Uversky, V. N. *Protein Sci.* **2002**, *11*, 739.
(17) Bitan, G.; Lomakin, A.; Teplow, D. B. *J. Biol. Chem.* **2001**, *276*, 35176.
(18) Teplow, D. B. Preparation of amyloid β-protein for structural and functional studies. *Amyloid, Prions, and Other Protein Aggregates, Pt C*; Elsevier Academic Press Inc: San Diego, CA, 2006; Vol. *413*, p 20.
(19) Ono, K.; Condron, M. M.; Teplow, D. B. *Proc. Natl. Acad. Sci. U.S.A.* **2009**, *106*, 14745.
(20) Lee, J. P.; Stimson, E. R.; Ghilardi, J. R.; Mantyh, P. W.; Lu, Y. A.; Felix, A. M.; Llanos, W.; Behbin, A.; Cummings, M.; Vancriekinge, M.; Timms, W.; Maggio, J. E. *Biochemistry* **1995**, *34*, 5191.
(21) Zhang, S.; Iwata, K.; Lachenmann, M. J.; Peng, J. W.; Li, S.; Stimson, E. R.; Lu, Y.; Felix, A. M.; Maggio, J. E.; Lee, J. P. *J. Struct. Biol.* **2000**, *130*, 130.
(22) Riek, R.; Guntert, P.; Dobeli, H.; Wipf, B.; Wuthrich, K. *Eur. J. Biochem.* **2001**, *268*, 5930.
(23) Hou, L. M.; Shao, H. Y.; Zhang, Y. B.; Li, H.; Menon, N. K.; Neuhaus, E. B.; Brewer, J. M.; Byeon, I. J. L.; Ray, D. G.; Vitek, M. P.; Iwashita, T.; Makula, R. A.; Przybyla, A. B.; Zagorski, M. G. *J. Am. Chem. Soc.* **2004**, *126*, 1992.
(24) Serpell, L. C. *Biochim. Biophys. Acta, Mol. Basis Dis.* **2000**, *1502*, 16.
(25) Wei, G. H.; Shea, J. E. *Biophys. J.* **2006**, *91*, 1638.
(26) Zanuy, D.; Ma, B. Y.; Nussinov, R. *Biophys. J.* **2003**, *84*, 1884.
(27) Klimov, D. K.; Thirumalai, D. *Structure* **2003**, *11*, 295.
(28) Favrin, G.; Irback, A.; Mohanty, S. *Biophys. J.* **2004**, *87*, 3657.
(29) Santini, S.; Wei, G. H.; Mousseau, N.; Derreumaux, P. *Structure* **2004**, *12*, 1245.
(30) Ma, B. Y.; Nussinov, R. *Proc. Natl. Acad. Sci. U.S.A.* **2002**, *99*, 14126.
(31) Balbach, J. J.; Ishii, Y.; Antzutkin, O. N.; Leapman, R. D.; Rizzo, N. W.; Dyda, F.; Reed, J.; Tycko, R. *Biochemistry* **2000**, *39*, 13748.
(32) Baumketner, A.; Shea, J. E. *J. Mol. Biol.* **2007**, *366*, 275.
(33) Melquiond, A.; Dong, X.; Mousseau, N.; Derreumaux, P. *Curr. Alzheimer Res.* **2008**, *5*, 244.
(34) Baumketner, A.; Shea, J. E. *J. Mol. Biol.* **2006**, *362*, 567.
(35) Baumketner, A.; Krone, M. G.; Shea, J. E. *Proc. Natl. Acad. Sci. U.S.A.* **2008**, *105*, 6027.
(36) Chebaro, Y.; Mousseau, N.; Derreumaux, P. *J. Phys. Chem. B* **2009**, *113*, 7668.
(37) Wise-Scira, O.; Xu, L.; Kitahara, T.; Perry, G.; Coskuner, O. *J. Chem. Phys.* **2011**, 135.
(38) Lazo, N. D.; Grant, M. A.; Condron, M. C.; Rigby, A. C.; Teplow, D. B. *Protein Sci.* **2005**, *14*, 1581.
(39) Baumketner, A.; Bernstein, S. L.; Wyttenbach, T.; Lazo, N. D.; Teplow, D. B.; Bowers, M. T.; Shea, J. E. *Protein Sci.* **2006**, *15*, 1239.
(40) Chen, W.; Mousseau, N.; Derreumaux, P. *J. Chem. Phys.* **2006**, *125*, 084911.
(41) Cruz, L.; Urbanc, B.; Borreguero, J. M.; Lazo, N. D.; Teplow, D. B.; Stanley, H. E. *Proc. Natl. Acad. Sci. U.S.A.* **2005**, *102*, 18258.
(42) Borreguero, J. M.; Urbanc, B.; Lazo, N. D.; Buldyrev, S. V.; Teplow, D. B.; Stanley, H. E. *Proc. Natl. Acad. Sci. U.S.A.* **2005**, *102*, 6015.
(43) Fawzi, N. L.; Phillips, A. H.; Ruscio, J. Z.; Doucleff, M.; Wemmer, D. E.; Head-Gordon, T. *J. Am. Chem. Soc.* **2008**, *130*, 6145.
(44) Murakami, K.; Irie, K.; Morimoto, A.; Ohigashi, H.; Shindo, M.; Nagao, M.; Shimizu, T.; Shirasawa, T. *J. Biol. Chem.* **2003**, *278*, 46179.
(45) Grabowski, T. J.; Cho, H. S.; Vonsattel, J. P. G.; Rebeck, G. W.; Greenberg, S. M. *Ann. Neurol.* **2001**, *49*, 697.
(46) Nilsberth, C.; Westlind-Danielsson, A.; Eckman, C. B.; Condron, M. M.; Axelman, K.; Forsell, C.; Stenh, C.; Luthman, J.; Teplow, D. B.; Younkin, S. G.; Naslund, J.; Lannfelt, L. *Nat. Neurosci.* **2001**, *4*, 887.
(47) Kamino, K.; Orr, H. T.; Payami, H.; Wijsman, E. M.; Alonso, M. E.; Pulst, S. M.; Anderson, L.; Odahl, S.; Nemens, E.; White, J. A.; Sadovnick, A. D.; Ball, M. J.; Kaye, J.; Warren, A.; McInnis, M.; Antonarakis, S. E.; Korenberg, J. R.; Sharma, V.; Kukull, W.; Larson, E.; Heston, L. L.; Martin, G. M.; Bird, T. D.; Schellenberg, G. D. *Am. J. Hum. Genet.* **1992**, *51*, 998.
(48) Vanbroeckhoven, C.; Haan, J.; Bakker, E.; Hardy, J. A.; Vanhul, W.; Wehnert, A.; Vegtervandervlis, M.; Roos, R. A. C. *Science* **1990**, *248*, 1120.
(49) Levy, E.; Carman, M. D.; Fernandezmadrid, I. J.; Power, M. D.; Lieberburg, I.; Vanduinen, S. G.; Bots, G.; Luyendijk, W.; Frangione, B. *Science* **1990**, *248*, 1124.
(50) Dahlgren, K. N.; Manelli, A. M.; Stine, W. B.; Baker, L. K.; Krafft, G. A.; LaDu, M. J. *J. Biol. Chem.* **2002**, *277*, 32046.

(51) Grant, M. A.; Lazo, N. D.; Lomakin, A.; Condron, M. M.; Arai, H.; Yamin, G.; Rigby, A. C.; Teplow, D. B. *Proc. Natl. Acad. Sci. U.S.A.* **2007**, *104*, 16522.
(52) Krone, M. G.; Baumketner, A.; Bernstein, S. L.; Wyttenbach, T.; Lazo, N. D.; Teplow, D. B.; Bowers, M. T.; Shea, J. E. *J. Mol. Biol.* **2008**, *381*, 221.
(53) Murray, M. M.; Krone, M. G.; Bernstein, S. L.; Baumketner, A.; Condron, M. M.; Lazo, N. D.; Teplow, D. B.; Wyttenbach, T.; Shea, J. E.; Bowers, M. T. *J. Phys. Chem. B* **2009**, *113*, 6041.
(54) Petkova, A. T.; Ishii, Y.; Balbach, J. J.; Antzutkin, O. N.; Leapman, R. D.; Delaglio, F.; Tycko, R. *Proc. Natl. Acad. Sci. U.S.A.* **2002**, *99*, 16742.
(55) Luhrs, T.; Ritter, C.; Adrian, M.; Riek-Loher, D.; Bohrmann, B.; Doeli, H.; Schubert, D.; Riek, R. *Proc. Natl. Acad. Sci. U.S.A.* **2005**, *102*, 17342.
(56) Flock, D.; Colacino, S.; Colombo, G.; Di Nola, A. *Proteins: Struct., Funct., Bioinf.* **2006**, *62*, 183.
(57) Sgourakis, N. G.; Yan, Y. L.; McCallum, S. A.; Wang, C. Y.; Garcia, A. E. *J. Mol. Biol.* **2007**, *368*, 1448.
(58) Yang, M. F.; Teplow, D. B. *J. Mol. Biol.* **2008**, *384*, 450.
(59) Mitternacht, S.; Staneva, I.; Hard, T.; Irback, A. *Proteins: Struct., Funct., Bioinf.* **2010**, *78*, 2600.
(60) Urbanc, B.; Cruz, L.; Yun, S.; Buldyrev, S. V.; Bitan, G.; Teplow, D. B.; Stanley, H. E. *Proc. Natl. Acad. Sci. U.S.A.* **2004**, *101*, 17345.
(61) Lam, A. R.; Teplow, D. B.; Stanley, H. E.; Urbanc, B. *J. Am. Chem. Soc.* **2008**, *130*, 17413.
(62) Urbanc, B.; Betnel, M.; Cruz, L.; Bitan, G.; Teplow, D. B. *J. Am. Chem. Soc.* **2010**, *132*, 4266.
(63) Anand, P.; Nandel, F. S.; Hansmann, U. H. E. *J. Chem. Phys.* **2008**, *128*, 165102.
(64) Baumketner, A.; Bernstein, S. L.; Wyttenbach, T.; Bitan, G.; Teplow, D. B.; Bowers, M. T.; Shea, J. E. *Protein Sci.* **2006**, *15*, 420.
(65) Sciarretta, K. L.; Gordon, D. J.; Petkova, A. T.; Tycko, R.; Meredith, S. C. *Biochemistry* **2005**, *44*, 6003.
(66) Sandberg, A.; Luheshi, L. M.; Sollvander, S.; de Barros, T. P.; Macao, B.; Knowles, T. P. J.; Biverstal, H.; Lendel, C.; Ekholm-Petterson, F.; Dubnovitsky, A.; Lannfelt, L.; Dobson, C. M.; Hard, T. *Proc. Natl. Acad. Sci. U.S.A.* **2010**, *107*, 15595.
(67) Ma, B. Y.; Nussinov, R. *Biophys. J.* **2006**, *90*, 3365.
(68) Hammarstrom, P.; Wiseman, R. L.; Powers, E. T.; Kelly, J. W. *Science* **2003**, *299*, 713.
(69) Jorgensen, W. L.; Madura, J. D. *Mol. Phys.* **1985**, *56*, 1381.
(70) Kaminski, G. A.; Friesner, R. A.; Tirado-Rives, J.; Jorgensen, W. L. *J. Phys. Chem. B* **2001**, *105*, 6474.
(71) Berendsen, H. J. C.; Vanderspoel, D.; Vandrunen, R. *Comput. Phys. Commun.* **1995**, *91*, 43.
(72) Lindahl, E.; Hess, B.; van der Spoel, D. *J. Mol. Model.* **2001**, *7*, 306.
(73) Berendsen, H. J. C.; Postma, J. P. M.; Vangunsteren, W. F.; Dinola, A.; Haak, J. R. *J. Chem. Phys.* **1984**, *81*, 3684.
(74) Miyamoto, S.; Kollman, P. A. *J. Comput. Chem.* **1992**, *13*, 952.
(75) Hess, B.; Bekker, H.; Berendsen, H. J. C.; Fraaije, J. *J. Comput. Chem.* **1997**, *18*, 1463.
(76) Essmann, U.; Perera, L.; Berkowitz, M. L.; Darden, T.; Lee, H.; Pedersen, L. G. *J. Chem. Phys.* **1995**, *103*, 8577.
(77) Bussi, G.; Donadio, D.; Parrinello, M. *J. Chem. Phys.* **2007**, 126.
(78) Marqusee, S.; Baldwin, R. L. *Proc. Natl. Acad. Sci. U.S.A.* **1987**, *84*, 8898.
(79) Sanner, M. F.; Olson, A. J.; Spehner, J. C. *Biopolymers* **1996**, *38*, 305.
(80) Humphrey, W.; Dalke, A.; Schulten, K. *J. Mol. Graphics* **1996**, *14*, 33.
(81) Frishman, D.; Argos, P. *Proteins* **1995**, *23*, 566.
(82) Daura, X.; Gademann, K.; Jaun, B.; Seebach, D.; van Gunsteren, W. F.; Mark, A. E. *Angew. Chem., Int. Ed.* **1999**, *38*, 236.
(83) Kumar, S.; Nussinov, R. *J. Mol. Biol.* **1999**, *293*, 1241.
(84) Ruscio, J. Z.; Fawzi, N. L.; Head-Gordon, T. *J. Comput. Chem.* **2010**, *31*, 620.
(85) Ball, K. A.; Phillips, A. H.; Nerenberg, P. S.; Fawzi, N. L.; Wemmer, D. E.; Head-Gordon, T. *Biochemistry* **2011**, *50*, 7612.
(86) Tarus, B.; Straub, J. E.; Thirumalai, D. *J. Mol. Biol.* **2008**, *379*, 815.
(87) Luttmann, E.; Fels, G. *Chem. Phys.* **2006**, *323*, 138.
(88) Munoz, V.; Thompson, P. A.; Hofrichter, J.; Eaton, W. A. *Nature* **1997**, *390*, 196.
(89) Karplus, M. *J. Phys. Chem. B* **2000**, *104*, 11.
(90) Ferrara, P.; Apostolakis, J.; Caflisch, A. *J. Phys. Chem. B* **2000**, *104*, 5000.
(91) Zheng, W. H.; Andrec, M.; Gallicchio, E.; Levy, R. M. *Proc. Natl. Acad. Sci. U.S.A.* **2007**, *104*, 15340.
(92) Zuckerman, D. M. Equilibrium sampling in biomolecular simulations. In *Annual Review of Biophysics*; Rees, D. C., Dill, K. A., Williamson, J. R., Eds.; Annual Reviews: Palo Alto, CA, 2011; Vol. *40*, p 41.
(93) Denschlag, R.; Lingenheil, M.; Tavan, P. *Chem. Phys. Lett.* **2008**, *458*, 244.
(94) Beck, D. A. C.; White, G. W. N.; Daggett, V. *J. Struct. Biol.* **2007**, *157*, 514.
(95) Antzutkin, O. N.; Leapman, R. D.; Balbach, J. J.; Tycko, R. *Biochemistry* **2002**, *41*, 15436.
(96) Hoyer, W.; Gronwall, C.; Jonsson, A.; Stahl, S.; Hard, T. *Proc. Natl. Acad. Sci. U.S.A.* **2008**, *105*, 5099.
(97) Reddy, G.; Straub, J. E.; Thirumalai, D. *J. Phys. Chem. B* **2009**, *113*, 1162.
(98) Walsh, D. M.; Lomakin, A.; Benedek, G. B.; Condron, M. M.; Teplow, D. B. *J. Biol. Chem.* **1997**, *272*, 22364.
(99) Eisenhauer, P. B.; Johnson, R. J.; Wells, J. M.; Davies, T. A.; Fine, R. E. *J. Neurosci. Res.* **2000**, *60*, 804.
(100) Tomidokoro, Y.; Rostagno, A.; Neubert, T. A.; Lu, Y.; Rebeck, G. W.; Frangione, B.; Greenberg, S. M.; Ghiso, J. *Am. J. Pathol.* **2010**, *176*, 1841.
(101) Van Nostrand, W. E.; Melchor, J. P.; Cho, H. S.; Greenberg, S. M.; Rebeck, G. W. *J. Biol. Chem.* **2001**, *276*, 32860.
(102) Bornebroek, M.; Haan, J.; Roos, R. A. C. *Amyloid-Int. J. Exp. Clin. Investig.* **1999**, *6*, 215.
(103) Paivio, A.; Jarvet, J.; Graslund, A.; Lannfelt, L.; Westlind-Danielsson, A. *J. Mol. Biol.* **2004**, *339*, 145.
(104) Whalen, B. M.; Selkoe, D. J.; Hartley, D. M. *Neurobiol. Dis.* **2005**, *20*, 254.
(105) Zameer, A.; Schulz, P.; Wang, M. S.; Sierks, M. R. *Biochemistry* **2006**, *45*, 11532.
(106) Legleiter, J.; Czilli, D. L.; Gitter, B.; DeMattos, R. B.; Holtzman, D. M.; Kowalewski, T. *J. Mol. Biol.* **2004**, *335*, 997.
(107) Liu, R. T.; Yuan, B.; Emadi, S.; Zameer, A.; Schulz, P.; McAllister, C.; Lyubchenko, Y.; Goud, G.; Sierks, M. R. *Biochemistry* **2004**, *43*, 6959.